PRECLINICAL AND CLINICAL SPECTROSCOPY – Full Paper

Magnetic Resonance in Medicine 80:29–35 (2018)

^{31}P T_2s of Phosphomonoesters, Phosphodiesters, and Inorganic Phosphate in the Human Brain at 7T

Wybe J.M. van der Kemp,* Dennis W.J. Klomp, and Jannie P. Wijnen

Purpose: To determine the phosphorus-31 T_2s of phosphomonoesters, phosphodiesters, and inorganic phosphate in the healthy human brain at 7T.

Methods: A 3D chemical shift imaging multi-echo sequence with composite block pulses for refocusing was used to measure one free induction decay (FID) and seven full echoes with an echo spacing of 45 ms on the brain of nine healthy volunteers (age range 22–45 years; average age 27 ± 8 years). Spectral fitting was used to determine the change in metabolic signal amplitude with echo time.

Results: The average apparent T_2s with their standard deviation were 202 ± 6 ms, 129 ± 6 ms, 86 ± 2 ms, 214 ± 10 ms, and 213 ± 11 ms for phosphoethanolamine, phosphocholine, inorganic phosphate, glycerophosphoethanolamine, and glycerophosphocholine, respectively.

Conclusion: The determined apparent T_2 for phosphoethanolamine, glycerophosphocholine, and glycerophosphoethanolamine is approximately 200 ms. The lower apparent T_2 value for phosphocholine is attributed to the overlap of this resonance with the 3-phosphorous resonance of 2,3-diphosphoglycerate from blood, with an apparent shorter T_2. Omitting the FID signal and the first echo of phosphocholine leads to a T_2 of 182 ± 7 ms, whereas a biexponential analysis leads to 203 ± 4 ms. These values are more in line with phosphoethanolamine and the phosphodiesters. The short T_2 of inorganic phosphate is subscribed to the fast reversible exchange with γ-adenosine triphosphate, which is mediated by glyceraldehyde-3-phosphate dehydrogenase and phosphoglycerate kinase within the glycolytic pathway. **Magn Reson Med 80:29–35, 2018.**

Key words: ^{31}P; healthy brain; T_2; CPMG; 7T; phosphomonoesters; phosphodiesters; inorganic phosphate

INTRODUCTION

In vivo phosphorous-31 (^{31}P) MR spectroscopy provides an in situ window on cell energy and phospholipid membrane metabolism. Because these processes are crucial in the development and sustenance of a healthy brain function, ^{31}P MR spectroscopy has been applied in the investigation of the healthy brain (1–3) and brain diseases such as schizophrenia (4,5), bipolar disorder (6–8), Alzheimer's disease (9,10), attention deficit hyperactivity disorder (11), Parkinson's disease (12), epilepsy (13,14), multiple sclerosis (15,16), and brain tumors (17–19).

Although ^{31}P MRS on clinical 1.5T MR systems is hampered by low signal-to-noise ratio (SNR) and low spatial, temporal, and spectral resolution, the development of human high field (3T) and ultrahigh field (7T) systems alleviates these restraints. However, the increased spectral resolution at 7T impairs the chemical shift range over which homogeneous radiofrequency (RF) excitation and refocusing can be performed. Additionally, ultrahigh field MR leads to more RF deposition as compared to MR at lower field strengths.

The first in vivo ^{31}P study of the human brain at 7T by Lei et al. (1) was published in 2003. In that study, the T_1 and T_2 of phosphocreatine (PCR) and adenosine triphosphate were determined. Accurate knowledge of MR relaxation parameters is essential in optimizing spectroscopy pulse sequences for repetition time and echo time (TE), and is required for absolute quantification of metabolites. In addition, relaxation properties may provide information about the molecular dynamics of metabolites and tissue susceptibilities.

Here we report on the T_2s of the ^{31}P metabolites in the chemical shift range of 2.9 to 6.9 parts per million (ppm), that is, the phosphodiesters (glycerophosphocholine (GPC) and glycerophosphoethanolamine (GPE)), inorganic phosphate (Pi), and the phosphomonoesters ((phosphocholine (PC) and phosphoethanolamine (PE)), using multi-echo acquisitions with incorporation of imperfections in flip angles. To the best of our knowledge, this is the first report on the T_2s of these metabolites in the human brain at 7T.

In previous work, we determined the T_2s of these metabolites in healthy breast tissue (20) and breast cancer tissue (21) at 7T. Of particular interest in these

Department of Radiology, University Medical Center Utrecht, Utrecht, The Netherlands.

Grant sponsor: Dutch Cancer Society, Alpe d'Huzes; Grant number: UU2013-6302; Grant sponsor: Dutch Scientific Organization; Grant number: VENI-JW-016.148.002.

*Correspondence to: Wybe J.M. van der Kemp, Department of Radiology, University Medical Center Utrecht, The Netherlands, P.O. Box 85500, 3508 GA Utrecht, The Netherlands. E-mail: w.j.m.vanderkemp@umcutrecht.nl

Received 20 July 2017; revised 3 November 2017; accepted 3 November 2017

DOI 10.1002/mrm.27026

Published online 7 December 2017 in Wiley Online Library (wileyonlinelibrary.com).

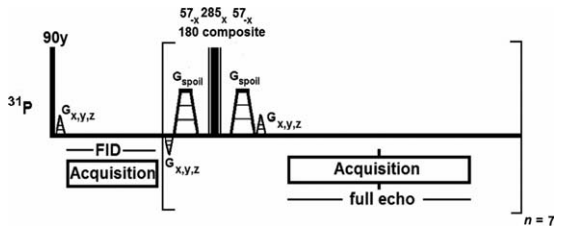

FIG. 1. Multi-echo spectroscopic imaging sequence with composite block pulses for refocusing, used in combination with a dual-tuned phosphorus-31–hydrogen-1 (^{31}P-^{1}H) birdcage head coil at 7T.

studies was a much shorter T_2 for Pi in breast cancer tissue than in healthy breast tissue, which we attribute to upregulated glycolysis in breast cancer tissue, causing reversible exchange between Pi and adenosine triphosphate (ATP). Because the glyceraldehyde-3-phosphate dehydrogenase (GAPDH) mRNA expression of the human cortex is among the tissues with the highest expression (22), and the GAPDH enzyme mediates this Pi–ATP exchange (22), we hypothesized to observe a short T_2 of Pi in the brain as well.

METHODS

Nine healthy volunteers who gave written informed consent were scanned on a 7T whole-body MR scanner (Philips, Best, The Netherlands) with a dual-tuned ^{31}P-^{1}H head coil (MR Coils BV, Zaltbommel, the Netherlands). The scan protocol consisted of basic imaging for positioning, B_0 map for image-based shimming with a shim tool (MR Code BV) based on FASTERMAP (23), and a ^{31}P flip-angle series (block pulses with step 15 degrees) in the nominal range 315 to 420 degrees to calibrate the flip angle in obtaining an actual flip of 360 degrees. After B_0 shimming and ^{31}P pulse calibration, a multi-echo 3D chemical shift imaging scan (Fig. 1) with spherical k-space sampling was performed (repetition time = 6 s; field of view = $280 \times 280 \times 280\,\text{mm}^3$; matrix = $8 \times 8 \times 8$; bandwidth = 7,000 Hz; 256 data points on a full echo; ΔTE = 45 ms; amplitude of (excitation) RF field (B_1) = 40 μT), acquiring one free induction decay (FID) and seven full echoes. Proton decoupling was not used because the in vivo spectral line width at 7T is larger than the scalar coupling constants.

The performance of the implemented multi-echo sequence, with composite block pulses for refocusing, was simulated using TopSpin 3.5 (Bruker, Billerica, Massachusetts, USA) and compared to a simulated multi-echo sequence with 180-degree block pulses for refocusing. Simulations were done without taking into account transverse or longitudinal relaxation effects. Deviations from perfect refocusing at the chemical shifts of the metabolites of interest were modeled with exponential decay. The simulated signals $S_{n,m}$ of the n echoes at chemical shift of metabolite m, were fitted to

$$S_{n,m}(n\Delta TE) = A_{0,m}\exp\left(\frac{-n\Delta TE}{T_{2,\text{pp},m}}\right), \quad [1]$$

where $T_{2,\text{pp},m}$ is a time constant that is dependent on the RF pulse performance (pp) at the chemical shift of metabolite m. With the $T_{2,\text{pp},m}$ obtained from simulations, the measured experimental volunteer data can be fitted to

$$S_{n,m}(n\Delta TE) = A^{*}_{0,m}\exp\left(\frac{-n\Delta TE}{T_{2,\text{pp},m}} - \frac{n\Delta TE}{T_{2,m}}\right). \quad [2]$$

The metabolite $T_{2,m}$ and the pp $T_{2,\text{pp},m}$ can be combined to an apparent metabolite $T_{2,m,\text{apparent}}$

$$\frac{1}{T_{2,m,\text{apparent}}} = \frac{1}{T_{2,m}} + \frac{1}{T_{2,pp,m}}. \quad [3]$$

Acquired ^{31}P data were spatially Hanning-filtered; FID data was first-order phased by circular shifting the first missing data points resulting from the delay between pulse and acquisition. All data were zero-filled in the time domain. After Fourier transform, the spectra were zero-order phase-corrected (based on the absolute full echo signal), and a baseline correction was applied to the FID spectrum to correct for the baseline rollover artefact as a result of the first missing data points. For each volunteer, one voxel was chosen for analysis. Because the nominal voxel size is $35 \times 35 \times 35\,\text{mm}^3$, the effective voxel size after Hanning filtering spans a large part of the brain. A voxel center location was central in the left–right and anteroposterior directions of the brain and a few

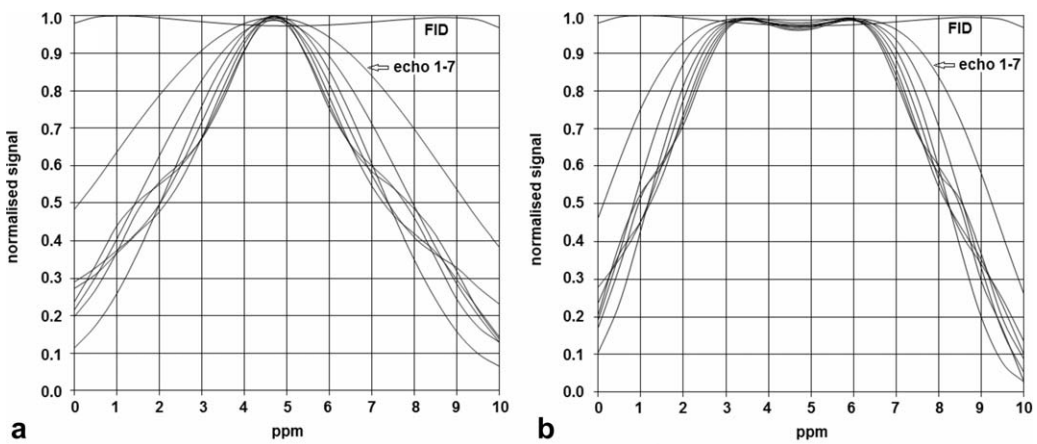

FIG. 2. Simulated signal for the free induction decay (FID) and the subsequent seven echoes of the multi-echo spectroscopic imaging sequence shown in Figure 1. (**a**) Refocusing with 180° block pulses; (**b**) refocusing with composite $57^{\circ}_{-x}285^{\circ}_{x}57^{\circ}_{-x}$ block pulses. The transmitter offset was 4.7 parts per million (ppm), and the amplitude of (excitation) radiofrequency (RF) field (B_1) = 40 μT.

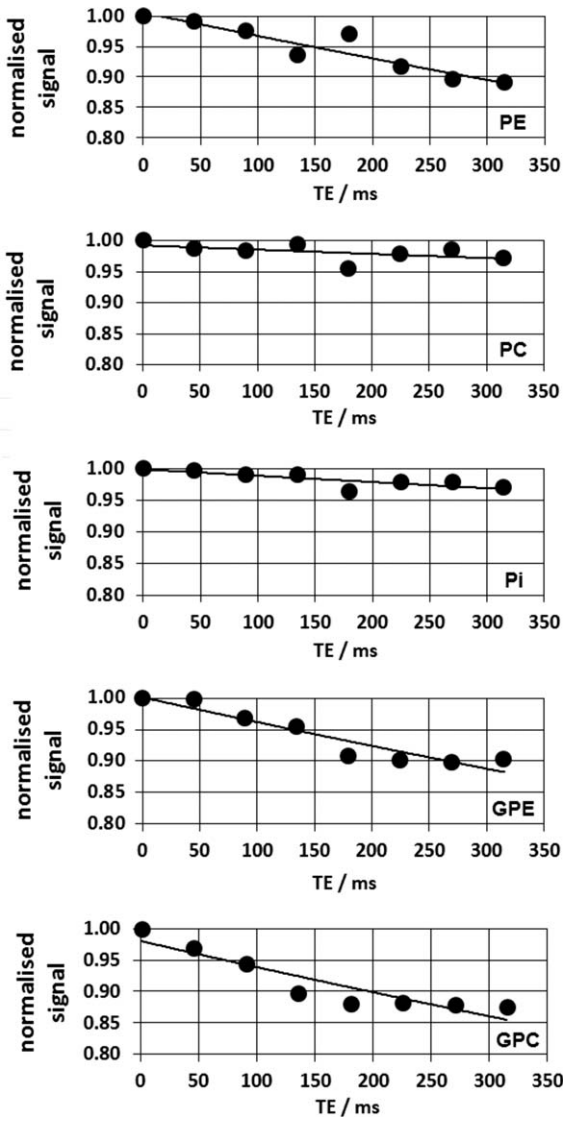

FIG. 3. Pulse performance (pp) time constants $T_{2,pp,m}$ fits to Equation [1] at the metabolite chemical shifts of phosphoethanolamine (PE), phosphocholine (PC), inorganic phosphate (Pi), glycerophosphoethanolamine (GPE), and glycerophosphocholine (GPC). RF pulses were on resonance at 4.7 ppm and with a $B_1 = 40\,\mu T$.

centimetres below the skull in a feet-head direction. This corresponds to the voxel with the highest SNR for optimal T_2 analysis. Spectral fitting was performed with jMRUI 5.2 (24) using the AMARES algorithm (25). Line widths of PE, PC, GPE, GPC were kept identical and free; and the line width of Pi was free. All metabolites were fitted using Gaussian line shapes. Chemical shift of metabolites was fixed within a 0.3 ppm range. After spectral fitting, the calculated amplitudes of the metabolites within FID and echoes were fitted to Equation [2]. The Cramér–Rao lower bounds of the spectral fitting were used as uncertainties in the exponential fitting with Equation [2]. The fitted T_2 values per metabolite and per volunteer were variance-weighted to obtain a best average T_2 value per metabolite. To enable the acquisition of seven echoes, the sampling times for FID and echo acquisitions were kept relatively short, leading to a small truncation artefact in the spectra. This artefact was removed (for viewing purpose only) by replacing the truncated tail of the experimental time domain data by the tail of the fitted time domain data obtained from jMRUI 5.2.

RESULTS

In Figures 2a,2b, the results for the simulations of the multi-echo sequence with 180-degree refocusing block pulses and refocusing composite block pulse are compared, respectively. It is clear that with 180-degree block pulses at $B_1 = 40\,\mu T$, the first echo already shows a drop in intensity to approximately 90%, within the 4-ppm range of interest of approximately 4.7 ppm. A better refocusing performance is seen with the composite block pulse, although a small drop in intensity can be observed, particularly on the edges of the 4-ppm range of interest.

Applying the multi-echo sequence with composite block refocusing pulses will lead to a small underestimation of the T_2 of metabolites, which can be corrected by taking into account the pp profile of Figure 2b, for which the deviation can be fitted as an exponential decay given by Equation [1]. The results of fitting the corrective pp time constants, $T_{2pp,m}$, at the different chemical shifts of the metabolites, are shown in Figure 3.

The numerical values of the pp time constants $T_{2,pp,m}$ in seconds, which were fitted at the different chemical shifts, are summarized in the second column of Table 1. An example of the chosen voxel localization for analysis, a full FID spectrum, and the multi-echo spectra in the chemical shift range 2 to 8 ppm for one volunteer are shown in Figure 4.

Because the refocusing bandwidth of the composite pulses is limited to approximately 4 ppm, only a small chemical shift range of the ^{31}P spectrum spanning the phosphodiesters and phosphomonoesters is shown for the multi-echo spectra. The T_2 fits of the different ^{31}P metabolites obtained from fitting the spectra at the different TEs for this volunteer are shown in Figure 5.

The truncation artifact that arises due to the relatively short TE (45 ms) and subsequent short sampling time (18.3 ms for the FID and 36.6 for a full echo) is illustrated in Figure 6. Figure 6a shows the spectrum of an almost fully sampled FID (55 ms sampling); Figure 6b shows the same spectrum but truncated after 18.3 ms (zero-filled to the original size); and Figure 6c shows the partial removal of the artifact (for viewing purpose) by using the tail of the FID as obtained by spectral fitting in jMRUI 5.2.

Table 1
Fitted Pulse Performance Time Constants, $T_{2,pp,m}$, of the Composite $57^\circ_{-x}285^\circ_{x}57^\circ_{-x}$ Block Pulse at 40 μT, Equation [1], at the Chemical Shift of the Different ^{31}P Metabolites, and Variance Weighted Metabolite T_2 Values Obtained From Nine Healthy Volunteers

Metabolite	$T_{2,pp,m}$/s	T_2,/ms
Phosphoethanolamine (PE)	2.6	202 ± 6
Phosphocholine (PC)	14.4	129 ± 6
Inorganic phosphate (Pi)	9.0	86 ± 2
Glycerophosphoethanolamine (GPE)	2.5	214 ± 10
Glycerophosphocholine (GPC)	2.3	213 ± 11

^{31}P, phosphorus-31; pp, pulse performance.

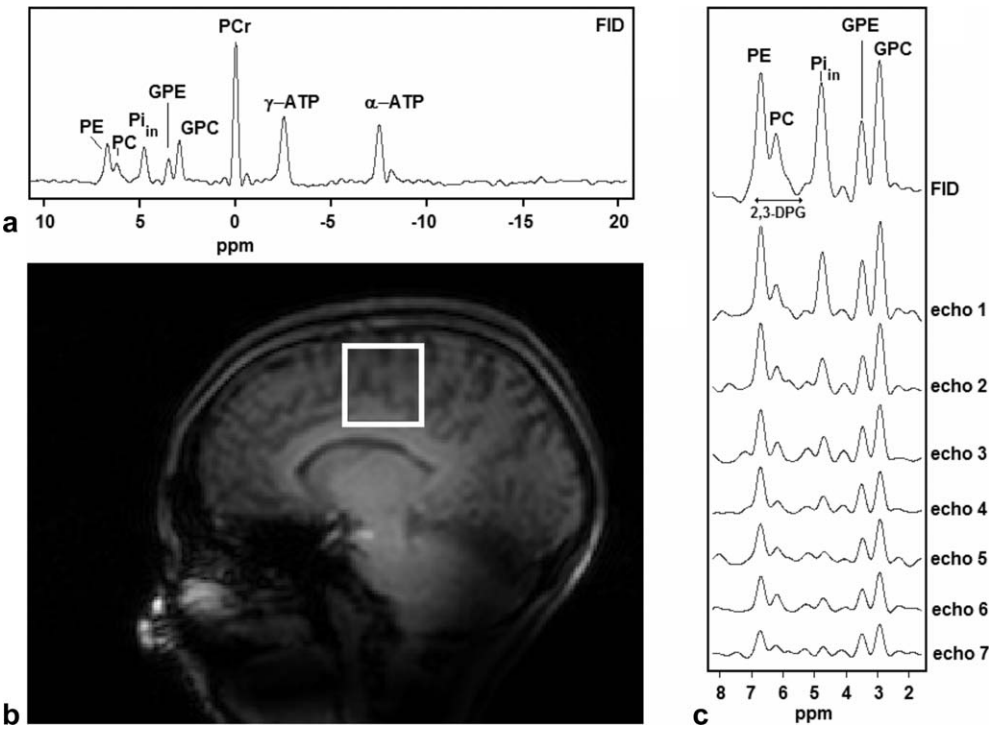

FIG. 4. (**a**) Scout image with chosen voxel in the brain of a healthy volunteer. (**b**) Full ^{31}P MRS spectrum derived from the 90° pulse acquired FID. Note the lack of β-adenosine triphosphate (β-ATP) signal due to limited excitation bandwidth. (**c**) Example of brain ^{31}P spectra (obtained from FID and echoes) from the selected voxel of this volunteer. The possible range of the chemical shift of the 2,3-diphosphoglycerate (2,3-DPG) signals, as indicated in the figure, is 5.4 to 6.9 ppm for $7.3 \leq pH_i \leq 7.4$ and $1\% \leq$ oxygenation $\leq 98\%$, respectively.

Averaged multi-echo spectra for the group of nine volunteers are shown in Figure 7.

An overview of all metabolite calculated T_2 values with the standard deviation of the fit for the nine subjects is shown in Figure 8. The last column in the graph shows the variance-weighted average of the metabolite T_2 over the nine volunteers. Numerical values of the variance-weighted averages of the metabolite transverse relaxation constants, T_2, are summarized in the third column of Table 1.

DISCUSSION

The determined time constants for correction of the pulse performance of the refocusing composite block pulse are in the range of 2.3 s to 14.4 s at the chemical shift of the metabolites investigated. With an intrinsic metabolic T_2 of 200 ms, this amounts to a correction that is in the range of 1% to 8%; however, with an intrinsic metabolic T_2 of 100 ms, the correction is only 1% to 4%.

The spectra derived from the FID and echo acquisitions, as depicted in Figure 4, clearly show signals from PE, PC, intracellular Pi (Pi_{in}), GPE, and GPC; however, there appear to be a few more signals visible. Due to the truncation artefact, it is difficult to distinguish between real signals and artefacts. The phosphomonoester signals (PE + PC) of the FID spectrum seem somewhat broadened. It is possible that two signals from 2,3-diphosphoglycerate (2,3-DPG), which is abundantly present in red blood cells, could contribute to the signal of PC, and to a lesser extent to PE in the FID spectrum. The visibility of these two ^{31}P signals from 2,3-DPG in the brain has been previously inferred (26,27). The chemical shift of the 2,3-DPG signals is highly dependent on the intracellular pH and the oxygenation of the red blood cells. For $7.3 \leq pH_i \leq 7.4$ and $1\% \leq$ oxygenation $< 98\%$, the chemical shift (referenced to PCr) of the 2P signal ranges from 5.4 to 6.2 ppm, whereas the chemical shift of the 3-phosphorous signal ranges from 6.2 to 6.9 (28–30). This spans the range of the phosphomonoesters PC and PE, with PC approximately 6.25 ppm and PE approximately 6.8 ppm. From a concentration perspective, 2,3-DPG from blood can contribute significantly to the signal of PC, although the impact of 2,3-DPG will probably be limited to the FID signal and possibly the first echo because the blood flow and the spoiler gradients around the refocusing pulses will dephase these signals substantially in the later echoes. Cerebral blood volume in healthy adults is approximately 3.8% of cerebral volume (31), whereas the normal 2,3-DPG concentration in packed red cells is 4.5 to 5.1 mM (32) and in normal haematocrit (males and females combined) is 36% to 50% (32). Combined, this leads to a cerebral 2,3-DPG concentration ranging from 0.061 to 0.099 mM. With two ^{31}P signals for one molecule of 2,3-DPG, the contributing signal to the PME signals is in the range of 0.12 to 0.2 mM. From autopsies, it is known that the normal concentration range of PC in the brain is 0.30 to 0.40 mM (33). Consequently, the PC signal as obtained by ^{31}P MRS could be 67% too high (upper limit) due to the contributing signals from 2,3-DPG.

The signal labeled Pi_{in} has a left shoulder of approximately 5.3 ppm that could be extracellular Pi. Extracellular phosphate in the brain has been identified previously by Ren et al. (2), who also measured the T_1 of the intracellular and extracellular phosphate signals in the brain. The origin of the signal at 4.3 ppm is not clear and is not confined to the spectra of the single volunteer in Figure 4. On averaging the spectra from all volunteers, this signal remains visible (Fig. 7). We are inclined to identify it as a truncation artefact, as shown in Figure 6; however,

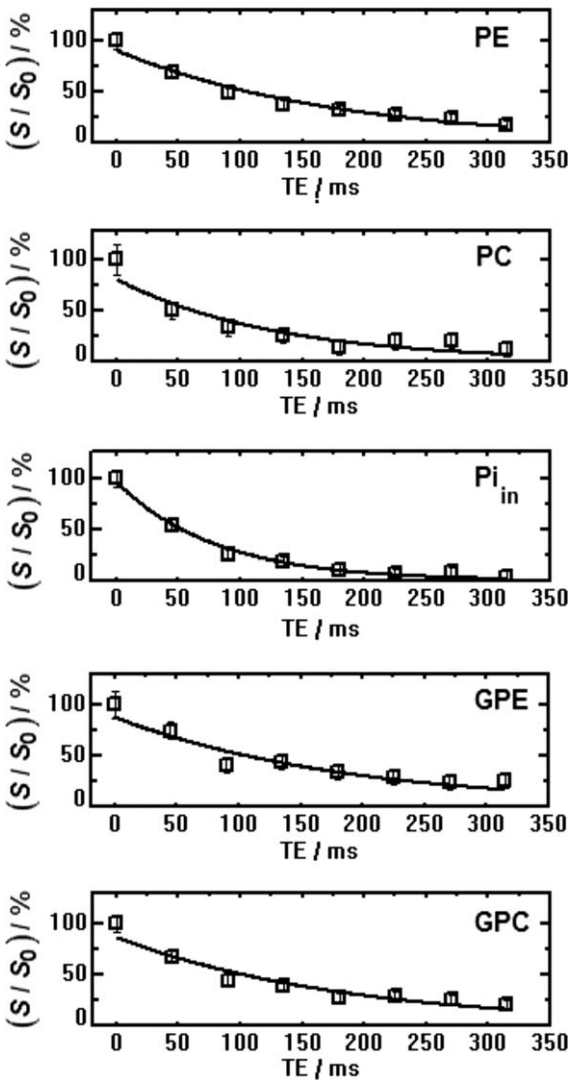

FIG. 5. T_2 Fits of the ^{31}P metabolites in the phosphodiester to phosphomonoester range of the data from the same volunteer, as shown in Figure 4. S/S_0 is relative signal intensity.

Pi in an acidic environment of pH of approximately 6.7 could possibly also explain the signal. Low pH values are not uncommon in, for instance, lysosomes; and a series of eight Pi signals at different pH have also been reported in the normal isolated dog brain, spanning the chemical shift range of 4.07 to 5.17 ppm (34).

The T_2s of PE, GPE, and GPC that were determined in the brain at 7T are comparable and approximately 200 ms. The apparent T_2 of PC is most likely too low because it is possibly influenced by the 3P and 2P signals of 2,3-DPG from blood, which have a shorter apparent T_2 than PC (due to blood flow and spoiler gradients around the refocusing pulses), as can be seen from the subsequent echo spectra in Figures 4 and 7. Upon omitting the FID and first echo signal for the T_2 fits of PC, a variance-weighted T_2 of 182 ± 7 ms is found. Fitting the T_2 of PC with a two-component model, taking into account a variable fraction of non-PC signal with a variable T_2, leads to a variance-weighted $T_2 = 203 \pm 4$ ms for PC. Here, we first determined an average T_2 and an average fraction for the underlying non-PC signal for the group of nine volunteers by fitting the individual PC data with the following constraints: 140 ms $\leq T_2$ (PC) $\leq$ 350 ms; fraction non-PC signal between 10% and 67%; and 0 ms $\leq T_2$ (non-PC) $\leq$ 75 ms. This leads to a fraction of non-PC signal of 52% and T_2 (non-PC) = 37 ms when averaged over all nine volunteers. These values were subsequently used, and fixed, to fit the individual T_2 data of PC for the nine volunteers. Variance weighting of these individual T_2s of PC then leads to the variance-weighted T_2 value of 203 ± 4 ms. These values are more in line with the T_2s of PE and the phosphodiesters.

Phosphorus spectroscopy, utilizing polarization transfer, indeed shows a much cleaner signal in the phosphomonoester range in the human brain because the underlying non-PC and non-PE signals are not amplified, as compared to a direct detection acquisition (35,36).

The rather short T_2 of Pi_{in} of only 86 ± 2 ms is likely caused by exchange with γ-ATP via the reversible reactions involving the GAPDH and phosphoglycerate kinase enzymes of the glycolytic pathway. It is known that GAPDH mRNA expression of the human cortex is high (22). The short T_2 time of Pi_{in} is corroborated by a short T_1, which was measured by Ren et al. (2), who found a 40% shorter T_1 for intracellular Pi as compared to extracellular Pi in the healthy human brain at 7T. These authors also attributed the shorter T_1 of Pi_{in} to exchange with γ-ATP. In addition, saturation transfer measurements in rat brain at 11.7T revealed that the extracellular inorganic phosphate Pi_{ex} is insensitive to saturating γ-ATP, whereas the signal of the intracellular pool Pi_{in} is

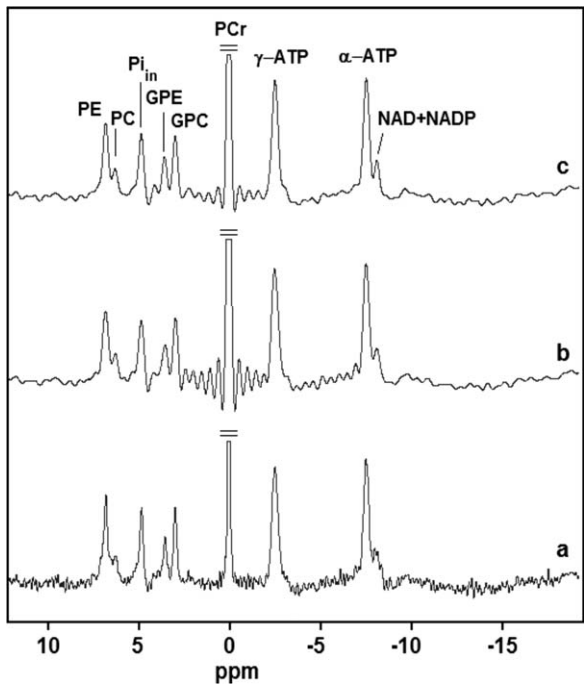

FIG. 6. (**a**) Example of a spectrum of an almost fully sampled FID (T_{acq} = 55 ms); (**b**) spectrum of a truncated FID (18.3 ms); and (**c**) spectrum of the truncated FID after filling the truncated time domain data with fitted data from jMRUI 5.2. All FIDs were zero-filled to the same number of points. NAD, nicotinamide adenine dinucleotide; NADP, nicotinamide adenine dinucleotide phosphate.

reduced, designating a cytosolic origin for exchange between Pi and γ-ATP (37). Note that saturation transfer measurements in skeletal muscle, with the aim of measuring the mitochondrial Pi to γ−ATP flux, always lead to extreme high values as compared to other methods (38). Here also, the cause is sought in the exchange between Pi and γ-ATP through the glycolytic pathway (38). Indeed, the T_2 of Pi_{in} from skeletal muscle is much shorter than, for instance, the T_2 of the phosphodiesters or PC (39,40) signals from skeletal muscle. Recently, we measured the T_2 of ^{31}P metabolites in healthy breast tissue and breast cancer tissue. For Pi in healthy breast tissue, we found 180 ± 4 ms (20), whereas the T_2 of Pi in breast cancer tissue was 87 ± 8 ms (21). Here, it also seems likely that the short T_2 of Pi in breast cancer tissue is caused by the exchange of Pi with γ-ATP via the glycolytic pathway because cancer cells have up-regulated glycolysis.

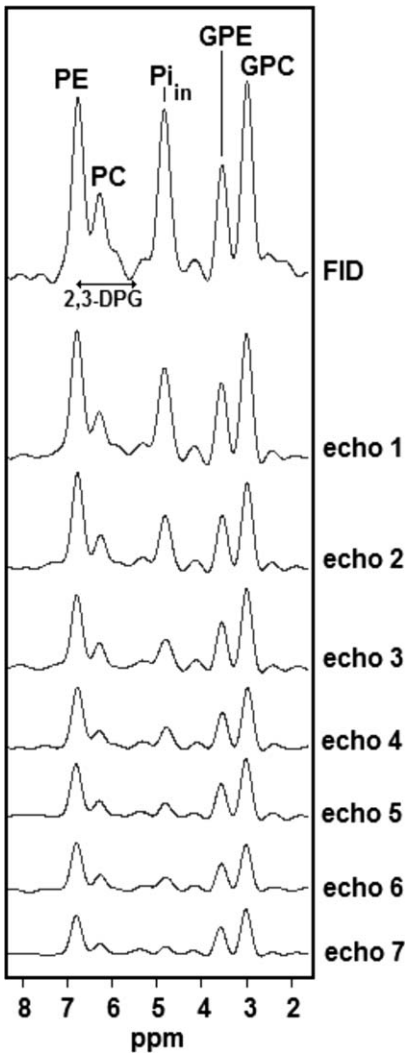

FIG. 7. Averaged brain ^{31}P MR spectra of the nine healthy volunteers (obtained from FID and echoes). For each volunteer, a voxel was chosen corresponding to the location, as shown in Figure 4a. The possible range of the chemical shift of the 2,3-DPG signals, as indicated in the figure, is 5.4 to 6.9 ppm for $7.3 \leq pH_i \leq 7.4$ and $1\% \leq$ oxygenation $\leq 98\%$, respectively.

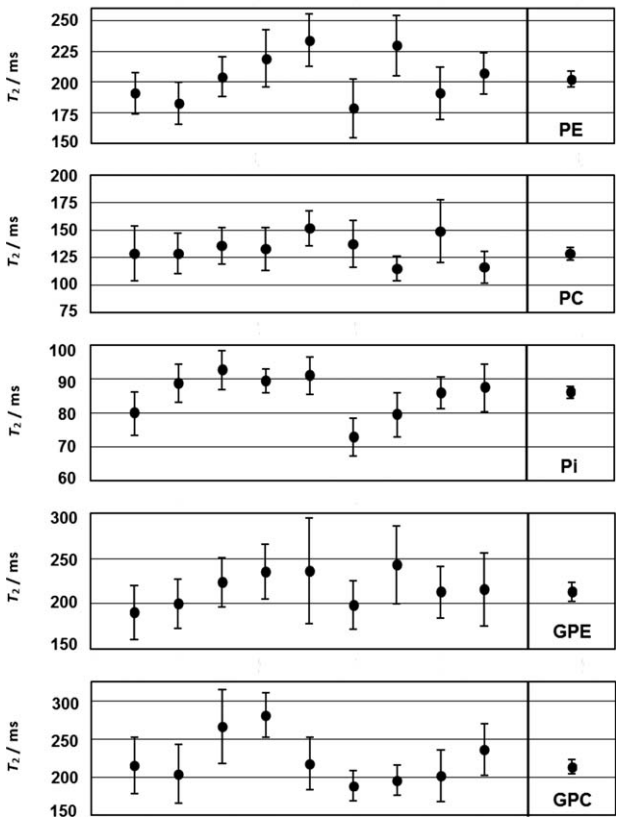

FIG. 8. Fitted T_2 Equation [2] values (standard deviation) of PE, PC, Pi, GPE, and GPC at 7T of the brain of nine healthy volunteers. The last plotted point for every metabolite is the variance weighted mean of the nine volunteers.

CONCLUSION

We determined the apparent T_2s of PE, GPC, and GPE to be approximately 200 ms and that of PC to be approximately 129 ms. We attribute the lower apparent T_2 value of PC to the overlap of this resonance with the 3P and 2P resonances of 2,3-DPG from blood, with a shorter T_2. Omitting the FID signal and the first echo of PC leads to a variance-weighted T_2 of 182 ± 7 ms, whereas a biexponential fit leads to a variance-weighted T_2 for PC of 203 ± 4 ms. The short T_2 of Pi of only 86 ms is subscribed to the fast reversible exchange with γ-ATP, which is mediated by GAPDH and phosphoglycerate kinase within the glycolytic pathway.

REFERENCES

1. Lei H, Zhu XH, Zhang XL, Ugurbil K, Chen W. In vivo 31P magnetic resonance spectroscopy of human brain at 7 T: an initial experience. Magn Reson Med 2003;49:199–205.
2. Ren J, Sherry AD, Malloy CR. (31)P-MRS of healthy human brain: ATP synthesis, metabolite concentrations, pH, and T1 relaxation times. NMR Biomed 2015;28:1455–1462.
3. Zhu XH, Lu M, Lee BY, Ugurbil K, Chen W. In vivo NAD assay reveals the intracellular NAD contents and redox state in healthy human brain and their age dependences. Proc Natl Acad Sci U S A. 2015;112:2876–2881.
4. Weber-Fahr W, Englisch S, Esser A, Tunc-Skarka N, Meyer-Lindenberg A, Ende G, Zink M. Altered phospholipid metabolism in schizophrenia: a phosphorus-31 nuclear magnetic resonance spectroscopy study. Psychiatry Res 2013;214:365–373.

5. Du F, Cooper AJ, Thida T, Sehovic S, Lukas SE, Cohen BM, Zhang X, Ongür D. In vivo evidence for cerebral bioenergetic abnormalities in schizophrenia measured using 31P magnetization transfer spectroscopy. JAMA Psychiatry 2014;71:19–27.
6. Kato T. Mitochondrial dysfunction in bipolar disorder: from 31P-magnetic resonance spectroscopic findings to their molecular mechanisms. Int Rev Neurobiol 2005;63:21–40.
7. Shi XF, Carlson PJ, Sung YH, et al. Decreased brain PME/PDE ratio in bipolar disorder: a preliminary 31P magnetic resonance spectroscopy study. Bipolar Disord 2015;17:743–752.
8. Du F, Yuksel C, Chouinard VA, Huynh P, Ryan K, Cohen BM, Öngür D. Abnormalities in high energy phosphate metabolism in first-episode bipolar disorder measured using 31P-magnetic resonance spectroscopy. Biol Psychiatry 2017. pii: S0006-3223(17)31466-X.
9. Pettegrew JW, Klunk WE, Panchalingam K, McClure RJ, Stanley JA. Magnetic resonance spectroscopic changes in Alzheimer's disease. Ann N Y Acad Sci 1997;826:282–306.
10. Mandal PK, Akolkar H, Tripathi M. Mapping of hippocampal pH and neurochemicals from in vivo multi-voxel 31P study in healthy normal young male/female, mild cognitive impairment, and Alzheimer's disease. J. Alzheimers Dis 2012;31(suppl 3):S75–S86.
11. Stanley JA, Kipp H, Greisenegger E, MacMaster FP, Panchalingam K, Pettegrew JW, Keshavan MS, Bukstein OG. Regionally specific alterations in membrane phospholipids in children with ADHD: an in vivo 31P spectroscopy study. Psychiatry Res 2006;148:217–221.
12. Rango M, Bonifati C, Bresolin N. Parkinson's disease and brain mitochondrial dysfunction: a functional phosphorus magnetic resonance spectroscopy study. J Cereb Blood Flow Metab 2006;26:283–290.
13. Kuzniecky R. Clinical applications of MR spectroscopy in epilepsy. Neuroimaging Clin N Am 2004;14:507–516.
14. Duncan JS. Imaging and epilepsy. Brain 1997;120:339–377.
15. Husted CA, Goodin DS, Hugg JW, Maudsley AA, Tsuruda JS, de Bie SH, Fein G, Matson GB, Weiner MW. Biochemical alterations in multiple sclerosis lesions and normal-appearing white matter detected by in vivo 31P and 1H spectroscopic imaging. Ann Neurol 1994;36:157–165.
16. Kauv P, Ayache SS, Créange A, Chalah MA, Lefaucheur JP, Hodel J, Brugières P. Adenosine triphosphate metabolism measured by phosphorus magnetic resonance spectroscopy: a potential biomarker for multiple sclerosis severity. Eur Neurol 2017;77:316–321.
17. Heindel W, Bunke J, Glathe S, Steinbrich W, Mollevanger L. Combined 1H-MR imaging and localized 31P-spectroscopy of intracranial tumors in 43 patients. J Comput Assist Tomogr 1988;12:907–916.
18. den Hollander JA, Luyten PR, Mariën AJ, Segebarth CM, Balériaux DF, de Beer R, van Ormondt D. Potentials of quantitative image-localized human 31P nuclear magnetic resonance spectroscopy in the clinical evaluation of intracranial tumors. Magn Reson Q 1989;5:152–168.
19. Ha DH, Choi S, Oh JY, Yoon SK, Kang MJ, Kim KU. Application of 31P MR spectroscopy to the brain tumors. Korean J Radiol 2013;14:477–486.
20. van der Kemp WJ, Stehouwer BL, Boer VO, Luijten PR, Klomp DW, Wijnen JP. Proton and phosphorus magnetic resonance spectroscopy of the healthy human breast at 7 T. NMR Biomed 2017;30:e3684.
21. van der Kemp WJM, van der Velden TA, Schmitz AM, Gilhuijs KG, Luijten PR, Klomp DWJ, Wijnen JP. Apparent short transverse relaxation time of inorganic phosphate in breast cancer tissue at 7 tesla. In Proceedings of the 25th Annual Meeting of ISMRM, Honolulu, Hawaii, USA, 2017. Abstract 0883.
22. Barber RD, Harmer DW, Coleman RA, Clark BJ. GAPDH as a housekeeping gene: analysis of GAPDH mRNA expression in a panel of 72 human tissues. Physiol Genomics 2005;21:389–395.
23. Shen J, Rycyna RE, Rothman DL. Improvements on an in vivo automatic shimming method [FASTERMAP]. Magn Reson Med 1997;38:834–839.
24. Naressi A, Couturier C, Devos JM, Janssen M, Mangeat C, de Beer R, Graveron-Demilly D. Java-based graphical user interface for the MRUI quantitation package. MAGMA 2001;12:141–152.
25. Vanhamme L, van den Boogaart A, Van Huffel S. Improved method for accurate and efficient quantification of MRS data with use of prior knowledge. J Magn Reson 1997;129:35–43.
26. Potwarka JJ, Drost DJ, Williamson PC. Quantifying 1H decoupled in vivo 31P brain spectra. NMR Biomed 1999;12:8–14. 27.
27. Harper DG, Plante DT, Jensen JE, Ravichandran C, Buxton OM, Benson KL, O'Connor SP, Renshaw PF, Winkelman JW. Energetic and cell membrane metabolic products in patients with primary insomnia: a 31-phosphorus magnetic resonance spectroscopy study at 4 tesla. Sleep 2013;36:493–500.
28. Labotka RJ. Measurement of intracellular pH and deoxyhemoglobin concentration in deoxygenated erythrocytes by phosphorus-31 nuclear magnetic resonance. Biochemistry 1984;23:5549–5555.
29. Petersen A, Kristensen SR, Jacobsen JP, Hørder M. 31P-NMR measurements of ATP, ADP, 2,3-diphosphoglycerate and Mg2 + in human erythrocytes. Biochim Biophys Acta 1990;1035:169–174.
30. Lam YF, Lin AK, Ho C. A phosphorus-31 nuclear magnetic resonance investigation of intracellular environment in human normal and sickle cell blood. Blood 1979;54:196–209.
31. Ito H, Kanno I, Kato C, et al. Database of normal human cerebral blood flow, cerebral blood volume, cerebral oxygen extraction fraction and cerebral metabolic rate of oxygen measured by positron emission tomography with 15O-labelled carbon dioxide or water, carbon monoxide and oxygen: a multicentre study in Japan. Eur J Nucl Med Mol Imaging 2004;31:635–643.
32. Bain BJ, Bates I, Laffan MA. Dacie and Lewis Practical Haematology. 12th ed. London, UK: Elsevier; 2017.
33. Komoroski RA, Pearce JM, Mrak RE. 31P NMR spectroscopy of phospholipid metabolites in postmortem schizophrenic brain. Magn Reson Med 2008;59:469–474.
34. Gilboe DD, Kintner D, Anderson ME, Fitzpatrick JH, Emoto SE, Markley JL. Inorganic phosphate compartmentation in the normal isolated canine brain. J Neurochem 1993;60:2192–2103.
35. Klomp DW, Wijnen JP, Scheenen TW, Heerschap A. Efficient 1H to 31P polarization transfer on a clinical 3T MR system. Magn Reson Med 2008;60:1298–1305.
36. Wijnen JP, Scheenen TW, Klomp DW, Heerschap A. 31P magnetic resonance spectroscopic imaging with polarisation transfer of phosphomono- and diesters at 3 T in the human brain: relation with age and spatial differences. NMR Biomed 2010;23:968–976.
37. Tiret B, Brouillet E, Valette J. Evidence for a "metabolically inactive" inorganic phosphate pool in adenosine triphosphate synthase reaction using localized 31P saturation transfer magnetic resonance spectroscopy in the rat brain at 11.7 T. J Cereb Blood Flow Metab 2016;36:1513–1518.
38. Kemp GJ, Brindle KM. What do magnetic resonance-based measurements of Pi→ATP flux tell us about skeletal muscle metabolism? Diabetes 2012;61:1927–1934.
39. Bogner W, Chmelik M, Andronesi OC, Sorensen AG, Trattnig S, Gruber S. In vivo 31P spectroscopy by fully adiabatic extended image selected in vivo spectroscopy: a comparison between 3 T and 7 T. Magn Reson Med 2011;66:923–930.
40. van der Kemp WJ, Boer VO, Luijten PR, Stehouwer BL, Veldhuis WB, Klomp DW. Adiabatic multi-echo ^{31}P spectroscopic imaging (AMESING) at 7 T for the measurement of transverse relaxation times and regaining of sensitivity in tissues with short T_2 values. NMR Biomed 2013;26:1299–1307.